A Novel GPER Antagonist Protects Against the Formation of Estrogen-Induced Cholesterol Gallstones in Female Mice

Chelsea DeLeon,[1] Helen H. Wang,[2] Joseph Gunn,[1] McKenna Wilhelm,[1] Aidan Cole,[1] Stacy Arnett,[3,#] David Q.-H. Wang,[2] Christopher K. Arnatt[1]

[1]Department of Chemistry, Saint Louis University, St. Louis, MO 63104, USA;

[2]Department of Medicine and Genetics, Division of Gastroenterology and Liver Diseases, Marion Bessin Liver Research Center, Einstein-Mount Sinai Diabetes Research Center, Albert Einstein College of Medicine, Bronx, NY 10461, USA; and

[3]Center for World Health and Medicine, Saint Louis University, St. Louis, MO 63104, USA

Address correspondence to:

Christopher K. Arnatt, Ph.D., Department of Chemistry, Saint Louis University, St. Louis, MO 63104, USA. Phone: (314) 977-8290, Fax: (314) 977-2521, Email: chris.arnatt@slu.edu

and

David Q.-H. Wang, M.D., Ph.D., Department of Medicine, Division of Hepatology, Marion Bessin Liver Research Center, Albert Einstein College of Medicine, Bronx, NY 10461, USA. Phone: (718) 430-8865, Fax: (718) 430-8568, Email: david.wang@einsteinmed.org

[#]Current address: Center for Clinical Pharmacology, Washington University, St. Louis, MO 63110

Downloaded from www.jlr.org by guest, on March 8, 2020

Abbreviations: CSI, cholesterol saturation index; DMSO, dimethyl sulfoxide; ERE, estrogen response elements; E_2, 17β-estradiol; ER, estrogen receptor; ERα, ER subtype α; ERβ, ER subtype β; FBS, fetal bovine serum; GPER1, G protein-coupled estrogen receptor 1; GPR30, G protein-coupled receptor 30; HTRF, homogeneous time-resolved fluorescence; OVX, ovariectomized.

Keywords: bile; bile salts; cholesterol crystallization; *Lith* gene; mucin; G protein-coupled estrogen receptor, GPER1, GPR30.

Downloaded from www.jlr.org by guest, on March 8, 2020

ASBMB JOURNAL OF LIPID RESEARCH

ABSTRACT

Many clinical studies and epidemiological investigations have clearly demonstrated that women are twice as likely to develop cholesterol gallstones as men, and oral contraceptives and other estrogen therapies dramatically increase that risk. Further animal studies revealed that estrogen promotes cholesterol gallstone formation through the estrogen receptor α (ERα), but not ERβ, pathway. More importantly, some genetic and pathophysiological studies found that the G protein-coupled estrogen receptor 1 (*Gper1*) is a new gallstone gene, *Lith18*, on chromosome 5 in mice and produces additional lithogenic actions, working independently of ERα, to markedly increase cholelithogenesis in female mice. Based upon computational modeling of GPER, a novel series of GPER-selective antagonists were designed, synthesized, and subsequently assessed for their therapeutic effects via calcium mobilization, cyclic AMP, and ERα and ERβ fluorescence polarization binding assays. From this series of compounds, one new compound, CIMBA, exhibits superior antagonism and selectivity exclusively for GPER. Furthermore, CIMBA reduces the formation of 17β-estradiol-induced gallstones in a dose-dependent manner in ovariectomized mice fed a lithogenic diet for 8 weeks. At 32 μg/day/kg of CIMBA, no gallstones are found in ovariectomized ERα (-/-) mice even treated with 17β-estradiol (6 μg/day) and fed the lithogenic diet for 8 weeks. In conclusion, CIMBA treatment protects against the formation of estrogen-induced cholesterol gallstones by inhibiting the GPER signaling pathway in female mice. This may provide a new effective therapy on cholesterol gallstone disease in women.

Downloaded from www.jlr.org by guest, on March 8, 2020

ASBMB JOURNAL OF LIPID RESEARCH

INTRODUCTION

Prior to the identification of the G protein-coupled estrogen receptor 1 (GPER), also known as the G protein-coupled receptor 30 (GPR30), the biological and physiological actions of estrogens were considered to originate exclusively from the nuclear estrogen receptors (ER), ERα and ERβ (1-3). Upon activation of the classical ER, individual ER subunits dimerize and bind to estrogen response elements (ERE) to directly regulate the expression of target genes (4-7). While the ER is primarily responsible for the genomic signaling, rapid, non-genomic signaling has been observed in response to estrogen. GPER was identified when there was the absence of both ERα and ERβ activation of mitogen-activated protein kinases 1 and 2 in response to 17β-estradiol (E_2) (8, 9). Since the identification of GPER as a novel ER, a variety of pathways have been studied, including second messengers (e.g., Ca^{2+} and cAMP), tyrosine kinase epidermal growth factor receptor, and protein/lipid kinases (e.g., protein kinase A, protein kinase C, and Src family) (10-14). Despite the affinity of E_2 for GPER, other estrogenic compounds such as 17α-estradiol, estrone, and estriol show little affinity for the receptor (**Figure 1**) and other hormones such as progesterone, testosterone, and cortisol exhibit no significant binding (15).

Several groups have identified GPER-selective agonists and antagonists (16-23). Using virtual screening and molecular docking of E_2-like compounds, Bologa and colleagues have found a GPER-selective agonist, G-1, that exhibits a binding constant (Ki) of 11 nM with no significant binding to ERα or ERβ at concentrations up to 1 μM (**Figure 1**) (16). Subsequently, two GPER-selective antagonists, G-15 and G-36, were identified based upon the same dihydroquinoline scaffold (17, 18). Although G-15 possessed a relative strong binding constant of 20 nM to GPER1, further studies revealed significant binding to the classical ER and

Downloaded from www.jlr.org by guest, on March 8, 2020

activation of ERE at concentrations above 100 nM (18). To address off-target binding and non-selectivity, Dennis *et al.* made modifications to the dihydroquinoline scaffold. As a result, G-36 was discovered. In this compound, the addition of a bulky, lipophilic group led to decreased binding to ER without significantly affecting activity at GPER (18). While decreased binding to the classical ER was reduced at concentrations above 1 μM, the ERE activation was still weakly present (18). These results show that the G-series GPER antagonists may be limited as GPER-selective antagonists due to the presence of off-target effects. Nevertheless, commercial availability of the G-series of ligands has made them valuable GPER chemical probes for research.

It is well known that the annual medical cost for treating gallstone disease exceeded $6 billion in 2004 and even higher in 2019 in the USA (24). The burden of gallstone disease is exacerbated by the fact that laparoscopic cholecystectomy remains the standard treatment for symptomatic gallstones worldwide (25). In addition, clinical and epidemiological studies have clearly demonstrated that women are twice as likely to develop cholesterol gallstones as men, and oral contraceptives or other estrogen therapies significantly increase that risk (26, 27). Although ERα, but not ERβ, plays a key role in estrogen's lithogenic effects (28), new evidence has shown that GPER can produce additional lithogenic actions, working independently of ERα, to promote gallstone formation in female mice (29, 30). More importantly, genetic analysis has found that *Gper1* is a new gallstone gene, *Lith18*, on chromosome 5 in mice (31). All these studies strongly suggested that GPER could play a critical role in the formation of estrogen-induced cholesterol gallstones (32).

To differentiate the GPER1-mediated effects from the ERα-mediated events in estrogen-induced cholesterol gallstones, we have created three knockout mouse lines: GPER1 (-/-), ERα (-

ASBMB JOURNAL OF LIPID RESEARCH

Downloaded from www.jlr.org by guest, on March 8, 2020

/-), and GPER1(-/-)/ERα(-/-) (29). Our results have shown that compared to ovariectomized (OVX) wild-type mice, deletion of either *Erα* or *Gper1* significantly reduced the prevalence of estrogen-induced gallstones, but could not abolish it completely. Furthermore, no gallstones were found in OVX GPER1(-/-)/ERα(-/-) mice even treated with E_2 at 6 μg/day and fed the lithogenic diet for 8 weeks (29). These results clearly indicated that GPER plays an independent role from ERα in the pathogenesis of cholesterol gallstone disease. Therefore, it is imperative to develop a new, potent GPER-selective antagonist that could prevent estrogen-induced gallstones for women.

Drug discovery for GPER ligands has been reliant upon the identification of individual ligands via *in silico* molecular screening, and only several synthetic GPER modulating molecules have been reported in the literature (16-23). However, there has been little effort from these studies to understand the important binding interactions of ligands within the binding pocket of GPER to aid in optimization. In this study, homology modeling was utilized to design and synthesize a series of GPER-selective antagonists (33, 34). Using calcium mobilization and cAMP assays, we have established the first series of compounds for exploring the importance of binding interactions for GPER-selective antagonists. Additionally, our animal studies have revealed that the lead compound discovered from this study can prevent the formation of E_2-induced cholesterol gallstones in OVX mice by inhibiting the GPER signaling pathway and may provide an additional effective therapeutic option for gallstone disease in women and patients exposed to high levels of estrogen.

JOURNAL OF LIPID RESEARCH ASBMB

Downloaded from www.jlr.org by guest, on March 8, 2020

MATERIALS AND METHODS

Chemistry

The compounds were synthesized according to the procedures shown in **Figure 2**. Characteristics of the compounds were analyzed utilizing nuclear magnetic resonance (NMR) and high-resolution mass spectroscopy. ^{1}H and ^{13}C NMR spectra were performed in chloroform-D from Cambridge Isotope Laboratories (Andover, MA) on a 400 MHz Bruker AVANCE III. Data was analyzed utilizing TopSpin 3.2 software. Experiments with high-resolution mass spectroscopy were carried out using a MaXis plus electrospray-quadrupole time-of-flight mass spectrometer (Bruker, Billerica, MA). Ionization was done by electrospray with the samples infused into the instrument in ~5 µM acetonitrile/water/formic acid (50/50/0.1%) solutions at a flow rate of 3 µl/minute. Nitrogen was used as nebulizing, drying, and collision gas. HPLC-grade acetonitrile and water were purchased from Sigma-Aldrich (St. Louis, MO). CIMBA exhibited a purity of greater than 95% as did all synthesized compounds. High-resolution mass spectroscopy for CIMBA ($C_{23}H_{32}NO^{+}$) was calculated as m/z = 338.2478 and found to be m/z = 338.2471.

Cell line and culture

The human promyelocytic leukemia (HL-60) cells, purchased from the American Type Culture Collection (Manassas, VA), were cultivated in phenol red-free RPMI 1640 media containing 10% heat-inactivated fetal bovine serum (FBS), 1% penicillin, and 1% GlutaMax. Three days prior to assays, the HL-60 cells were switched into the media containing 10% charcoal-stripped FBS. Cells were passaged every 3 days and maintained at a cell concentration below $1x10^{6}$ to prevent differentiation. The cells were incubated at 37°C under 5% CO_2.

Downloaded from www.jlr.org by guest, on March 8, 2020

ASBMB JOURNAL OF LIPID RESEARCH

Evaluation of GPER-associated calcium mobilization in HL-60 cells

The HL-60 cells were grown in 10% charcoal-stripped FBS, phenol red-free RPMI 72 hours before assays were performed. The cells were centrifuged and counted with a hemocytometer. The assay required 100,000 cells per well, for a total number of cells on a 96-well plate assay of about $1x10^7$. HL-60 cells ($1x10^7$) were incubated in 50:1 HBSS/HEPES containing 5 μM Indo-1 AM (Thermo Fisher Scientific, Waltham, MA) and 0.05% pluronic acid for 0.5 hours at room temperature. Cells were spun down and washed with 50:1 HBSS/HEPES and resuspended in media. Resuspension was placed on ice for no longer than 5 minutes. Cells were loaded into the plate at 100,000 cells/well. For agonist, cells were immediately incubated for 15 minutes at 37°C. Following the 15 minutes of incubation, FlexStation 3 Multimode Plate Reader (Molecular Devices, Sunnyvale, CA) added the appropriate amount of agonist and was read for 150 seconds at 37°C. For antagonists, once the cells were seeded, the antagonist was added and incubated for 15 minutes at 37°C. After 15 minutes of equilibration, the experimentally determined EC_{80} value of G-1 (3 μM) was added by the FlexStation and read for 150 secs at 37°C. Calcium mobilization was determined ratiometrically using λ_{ex} 350 nm and λ_{em} 405/490 nm, respectively.

Evaluation of cAMP response in HL-60 cells

A homogeneous time-resolved fluorescence (HTRF) components for cAMP was purchased from CisBio (Bedford, MA). HL-60 cells were grown in 10% charcoal-stripped FBS, phenol red-free RPMI media for 72 hours prior to assays. Cells were centrifuged and counted with a hemocytometer. The total number of cells needed to complete the assay was determined

Downloaded from www.jlr.org by guest, on March 8, 2020

based upon 8,000 cells/well. The determined number of cells was diluted in 5:1 (5x) stimulation buffer containing 500 µM of 3-isobutyl-1-methylxanthine (Sigma Aldrich, St. Louis, MO). To an HTRF 96-well low volume white plate from CisBio (cat:62AMgPEB), 5 µl of cold cell suspension was added to each well, followed by 4 µl of (2.5x) of agonist or stimulation buffer (negative control and non-stimulated cells). Cells were covered with a clear plastic film and incubated at 37°C for 15 minutes in an incubator. After 15 minutes, 1 µl of 10 µM (10x) forskolin was added to each well. The plate was once again sealed and incubated at 37°C for 15 minutes. Subsequently, 5 µl of cAMP-d_2 (acceptor) was added to all wells, including controls. Conversely, 5 µl of monoclonal anti-cAMP $Eu3^+$ cryptate (donor) was added to only the wells with a test compound and non-stimulated cells. Following the addition, the plate was sealed, covered with aluminum foil, and incubated at room temperature for 30 minutes. After the allotted time cells were read using Flexstation3 with λ_{ex} 314 nm and dual-emission wavelengths for the acceptor and donor emission signals ($\lambda_{em\ donor}$ = 620 nm and $\lambda_{em\ acceptor}$ = 655 nm). A ratio of the acceptor to the donor was calculated and utilized in the determination of EC_{50} value of G-1. For an antagonism platform, the procedure was slightly altered. The EC_{80} value of G-1 was re-determined based upon cAMP agonism results. To the plate, 2 µl of (5x) antagonist were added, followed by the addition of 5 µl of the cold cell suspension to all wells, with top and bottom wells being designated as G-1 control and forskolin control (20 µM), respectively. Cells and antagonists were incubated for 15 minutes at 37°C. Then, 2 µl of the (5x) EC_{80} of G-1 was added to wells with the antagonist. For the G-1 control, 2 µl of 5:1 stimulation buffer and 2 µl of the (5x) EC_{80} G-1 were added. For the forskolin control, 4 µl of 5:1 stimulation buffer and 1 µL of (10x) forskolin were combined. For all other wells, following the addition of antagonists, cells, and agonists, 1 µl of (10x) forskolin were add for a final concentration of 1 µM. After the

Downloaded from www.jlr.org by guest, on March 8, 2020

JOURNAL OF LIPID RESEARCH ASBMB

addition of forskolin, cells were incubated at 37°C for 5 minutes before dyes and lysis buffer were added. Cells were allowed to equilibrate for 30 minutes at room temperature before being read at λ_{ex} 314 nm dual-emission wavelengths for the acceptor and donor emission signals ($\lambda_{em\ donor}$ = 620 nm and $\lambda_{em\ acceptor}$ 655 = nm). A ratio of the acceptor to donor was calculated and utilized to determine the IC_{50} values of tested antagonists. HTRF values were converted to % cAMP using the manufacturer's suggested protocol.

ERα and ERβ fluorescence polarization assay

The ERα and ERβ PolarScreen Competitor Assays were purchased from Invitrogen (Carlsbad, CA). The concentrations of the ERα and ERβ enzymes varied between the two assays. A 4x sample of ERα was prepared for a final concentration of 75 nM. Conversely, a 4x sample of ERβ was prepared for a final concentration of 23 nM within the assay. For both ERα and ERβ, a 4x aliquot of Fluoromone was prepared for a final assay concentration of 4.5 nM. Despite the differences in concentration of ERα and ERβ, the binding assay protocol for the two different receptors remained the same. Drug dilutions were prepared for a 2x dilution in the ER-specific buffer that was provided within the assay kit. In addition to the drug dilutions, a 2x aliquot of Fluoromone was prepared by adding 10 µl of 4x with 10 µl of ER-specific buffer. A 2x dilution of enzyme and fluorophore was achieved by adding equal portions of each to each other. To a black 384-plate well plate, 10 µl of the compound was added to the wells, followed by 10 µl of the 2x mixture of enzyme and fluoromone. Two controls were included in the plate design. In one control, enzyme and compound were omitted so that only ER-specific buffer and fluoromone remained. A separate control contained the enzyme and fluoromone control. Once all components were added, the plate was covered with a film and aluminum foil. The plate was

ASBMB JOURNAL OF LIPID RESEARCH

Downloaded from www.jlr.org by guest, on March 8, 2020

incubated for 2 hours at room temperature before being read with λ_{ex} 485 nm and λ_{em} 535 nm, respectively.

Animal and diet

Although it has been found that inbred AKR/J mice are a gallstone-resistant strain, they are still susceptible to E_2-induced cholesterol gallstone formation (28). Although AKR/J mice have an intact expression of the *Gper1*, *Erα*, and *Erβ* genes, mRNA levels of *Erβ* in the liver are almost undetectable under normal physiological conditions. Hepatic expression of *Erβ* is 50-fold lower than that of *Erα* even under the stimulation of E_2. In addition, we have established breeding colonies of ERα (+/-) mice on an AKR/J genetic background in-house. ERα (+/-) heterozygotes were also fertile and showed no obvious phenotypes in association with the disrupted *Erα* genotype. A cross between heterozygous ERα (+/-) mice produced the live birth of normal litter sizes of homozygous ERα (-/-) mice. Mice were maintained in a temperature-controlled room (22±1°C) with a 12-hour day cycle (lights on 0600 h - 1800 h) and were provided free access to water and normal mouse chow containing trace cholesterol (<0.02%) (Lab Rodent Diet, St. Louis, MO). To exclude possible interindividual differences in endogenous estrogen concentrations, all female mice, at the age of 4 weeks, were ovariectomized (OVX). At 8 weeks of age, these mice were implanted subcutaneously with pellets (Innovative Research of America, Sarasota, FL) releasing 17β-estradiol (E_2) at 6 μg/day for 8 weeks. As reported (28), plasma estradiol concentrations were significantly increased to 81±21 pg/ml in OVX mice treated with E_2 at 6 μg/day compared to wild-type mice (26±11 pg/ml) receiving neither surgery nor E_2 treatment. To study the role of the GPER-selective antagonist CIMBA in the prevention of E_2-induced cholesterol gallstones, the mice, at 8 weeks old, were injected intraperitoneally

Downloaded from www.jlr.org by guest, on March 8, 2020

ASBMB JOURNAL OF LIPID RESEARCH

with CIMBA at 0, 16, or 32 μg/day/kg, as well as fed the lithogenic diet containing 1% cholesterol, 15% butter fat, and 0.5% cholic acid for 8 weeks. All procedures were in accordance with current NIH guidelines and were approved by the Institutional Animal Care and Use Committees of Albert Einstein College of Medicine (Bronx, NY) and Saint Louis University (St. Louis, MO).

Gallstone studies

After 8 weeks of feeding the lithogenic diet, mice were fasted overnight but had free access to water. After anesthetization with pentobarbital, cholecystectomy was performed during laparotomy. The entire gallbladder bile was studied by polarizing light microscopy without a cover slip and then with a cover slip using phase contrast optics for the presence of mucin gels, liquid crystals, cholesterol monohydrate crystals, sandy stones, and real gallstones according to previously established criteria (35). The images of cholesterol monohydrate crystals and gallstones were analyzed by a Carl Zeiss Imaging System with an AxioVision Rel 4.6 software (Carl Zeiss Microimaging GmbH, Göttingen, Germany). Under the circumstances, gallstones exhibit rounded contours and black centers from light scattering/absorption, and gallstones were counted at x100 or x200 magnification. The prevalence rate of gallstones is determined by the number of mice per group with evident stones. After microscopic studies, gallbladder bile was collected, frozen and stored at -20°C for lipid studies.

Biliary lipid analysis

Cholesterol, phospholipid, and bile salt concentrations in pooled gallbladder bile (n=10 mice per group) were determined according to previously published methods (36). Cholesterol

Downloaded from www.jlr.org by guest, on March 8, 2020

ASBMB JOURNAL OF LIPID RESEARCH

saturation index (CSI) of pooled gallbladder bile was calculated from critical tables (37) that was established for taurocholate, the predominant bile salts in the bile of mice on the lithogenic diet (38). Relative lipid composition of pooled gallbladder bile was plotted on condensed phase diagrams. For phase analysis, the phase limits of the micellar zones and the crystallization pathways were extrapolated from model bile systems developed for taurocholate at 37°C and at a total lipid concentration of ~10 g/dl (39).

Quantitative real-time PCR assay

Total RNA was extracted from fresh liver tissues of mice (n=4 per group) according to our published methods (29). Primer Express Software (Applied Biosystems, Foster City, CA) was used to design the primers based on sequence data available from GenBank. Quantitative real-time PCR assays of the hepatic *Gper1*, *Erα*, and *Erβ* genes were performed in triplicate according to previously established methods (29). The sequences of the primers for these genes have been reported (29). Relative mRNA levels were calculated using the threshold cycle of an unknown sample against a standard curve with known copy numbers. To obtain a normalized target value, the target amount was divided by the endogenous reference amount of mouse *β-Actin* as internal control.

Liver compound accumulation study

After liver samples were collected from mouse gallstone experiments, they were immediately frozen and stored at -80°C until analysis. Liver tissues were weighed and stored in Eppendorf tubes. Corresponding liver tissues were used for preparing standard curves in a tissue matrix. To each tissue sample or standard, the appropriate volume of cold PBS was added to

Downloaded from www.jlr.org by guest, on March 8, 2020

JOURNAL OF LIPID RESEARCH ASBMB

achieve a tissue concentration of 200 mg/ml. Stainless steel beads (2-3 mm) were added to the tubes that were then placed in a bead beater for 1-2 minutes. Tissue samples and standards (100 µl) were then added to a 96-well plate. Standards (100 µl) were also added to a separate 96-well plate. To each tissue well, 400 µl of cold acetonitrile containing 100 ng/ml internal standard enalapril was added. Plates were vortexed for 5 minutes at 4°C, then centrifuged at 3,200 rpm at 4°C for 10 minutes. The supernatant (400 µl) was transferred to a second 96-well plate, and evaporated to dryness under nitrogen, as well as reconstituted with 100 µl of 0.1% formic acid in water/acetonitrile (9:1, vol/vol), and vortexed for 5 minutes. After that, the samples were briefly centrifuged and submitted for LC/MS analysis. Compound concentrations were determined on a Sciex API-4000 LC/MS system in positive electrospray mode. Analyses were eluted from an Amour C18 reverse phase column (2.1x30 mm, 5 µm) using a 0.1% formic acid (aqueous) to 100% acetonitrile gradient mobile phase system at a flow rate of 0.35 ml/minute. Peak areas for the specific mass transitions were integrated using Analyst 1.5.1 software. Peak area ratios of analyses to the internal standard were plotted against concentration with a 1/x-weighted linear regression to determine compound concentration.

Statistical methods

All data are expressed as means ± SD. Statistically significant differences among groups of E_2-treated OVX mice fed the lithogenic diet and administrated with various doses of CIMBA were assessed by Student's *t*-test, or Chi-square tests, or by Mann-Whitney U-test. The 50% excitatory (EC_{50}) and 50% inhibitory concentrations (IC_{50}) were determined by nonlinear regression analysis using GraphPad Prism, version 5.02 (GraphPad, La Jolla, CA). All *ANOVA*

Downloaded from www.jlr.org by guest, on March 8, 2020

JOURNAL OF LIPID RESEARCH ASBMB

analyses were also run using the same statistical software with Tukey's post hoc analysis for multiple comparisons. Statistical significance was defined as a two-tailed probability of <0.05.

ASBMB JOURNAL OF LIPID RESEARCH

Downloaded from www.jlr.org by guest, on March 8, 2020

RESULTS

Design and synthesis of the GPER-selective antagonists, as well as inhibition of calcium mobilization and cAMP $G_{i/o}$ signaling by the GPER antagonists 5–25

Previous docking studies revealed the potential importance of hydrogen bonding to N310$^{7.40}$ (Ballesteros-Weinstein numbering) and E275$^{6.52}$, π-π stacking with F208 (extracellular loop 2, EL2) and H307$^{7.37}$, and various hydrophobic interactions with an extensive hydrophobic pocket (33). For this work, a scaffold was designed, as shown in **Figure 2A** (34). The synthetic route that was utilized in the synthesis of the GPER-selective antagonists is summarized in **Figure 2B**.

To assess the therapeutic efficacy of the synthesized GPER-selective antagonists, the human promyelocytic leukemia (HL-60) cell line was utilized because it displays high expression of *GPER1* in addition to both *ERα* and *ERβ*. Thus, using the HL-60 cells, off-target signaling was analyzed with a fluorescence polarization assay that will be discussed later. Prior to running antagonism assays, compounds **5**–**25** were tested for GPER agonism in a similar fashion as G-1, and no compounds showed agonism below 10 μM. Within the antagonism assay, nearly every compound exhibited an IC_{50} value in the high nanomolar range (**Table 1**). For comparison purposes, we determined that within the assay, the IC_{50} values of G-15 and G-36 were 1,550 ± 170 nM and 1,350 ± 220 nM, respectively. The previously reported calcium mobilization IC_{50} values of G-15 and G-36 varied from the determined values within this study. For G-15, the reported IC_{50} value was 185 nM, whereas the G-36 exhibited slightly greater potency with an IC_{50} value of 165 nM (18). Variation in the reported and observed IC_{50} values for G-15 and G-36 may exist due to differences in antagonism assay methodology between the study that reported these values and our study. For antagonism assays, Dennis *et al.* utilized 200

ASBMB JOURNAL OF LIPID RESEARCH

Downloaded from www.jlr.org by guest, on March 8, 2020

nM of G-1 to antagonize against G-15 and G-36 because there was a similar amount of calcium mobilization in SKBr3 cells for both E_2 and G-1 at this concentration (18). Standard methodology suggests that the standard method for performing an antagonism assay requires the $EC_{80/90}$ value of the agonist to create the necessary signal window for detecting inhibitory response (40, 41). While the EC50 value of G-1 has been reported in the literature, based upon this methodology it is unclear whether 200 nM truly represents the EC50/80 value of G-1. In the HL-60 cell line, the EC80 value was determined (data not shown) in a dose-dependent manner and existed at approximately 3 μM. Using 3 μM as the EC80 value of G-1, there was an approximate 10-fold magnitude difference in the IC50 values obtained in this study as compared to the literature for selective GPER antagonists, G-15 and G-36. This observed difference was approximately the same fold magnitude between the different values of G-1 (200 nM in the previous study (18) vs. 3 μM in this study) used to agonize the cells in the individual studies. Differences amongst the determined EC_{50} values may also exist due to the difference in expression levels of endogenous GPER between the cell lines.

The results from the calcium mobilization data revealed several key interactions of antagonists with GPER. In this series of compounds (**5**–**25**), the R_1 substitution greatly impacted GPER antagonism. Larger hydrophobic groups (isopropyl and *tert*-butyl) were well tolerated at R_1 position, whereas the methyl-substituted compounds (**12**–**18**) exhibited the lowest antagonism activity. For the R_1 substitution, isopropyl derivatives (**5**–**11**) had lower IC_{50} values than the *tert*-butyl derivatives (**19**–**25**). Overall, this suggests that small molecules may be limited in size due to restriction within the GPER binding pocket. Changes in activity observed by various R_2 substitutions were less straightforward. While mono-substitution appears to be favored over 3-4-disubstitution (**11**, **18**, and **25**), there was an insufficient number of compounds to verify whether

JOURNAL OF LIPID RESEARCH ASBMB

Downloaded from www.jlr.org by guest, on March 8, 2020

the 3- or 4-position confers favorable binding. The larger R_2 substituents such as naphthyl or biphenyl (**5**, **6**, **12**, **13**, **19**, and **20**) had mixed tolerances based upon the R_1 substitution. Differences in these observations may exist due to the size of the GPER binding pocket or the existence of different binding modes. The 4-Cl derivatives (**10**, **17**, and **24**) were unaffected by the R_1 substitution, whereas the other small substituents were all affected by the R_1 substitution. The two compounds with the lowest IC_{50} values, **8** (R_1 = isopropyl, R_2 = 4-OMe) and **21** (R_1 = *tert*-butyl, R_2 = 4-CH_3), had different substitution patterns and illustrated the potential for further optimization in future studies. These results were further verified in a secondary HTRF cAMP assay (**Figure 3A**). In this assay, HTRF was inversely proportional to cellular levels of cAMP. Accordingly, it was observed that G-1 increased HTRF signal, which indicated a decrease in the level of cAMP. Blocking GPER with an antagonist exhibited a decrease in HTFR signal, which corresponded to an increase in cAMP levels. Presented data shows % cAMP, which was calculated using the manufacturer's suggested protocol. Cellular response to G-1 was reversed with treatment of pertussis-toxin (1 μM), suggesting that G-1 signals through the $G_{i/o}$ pathway (**Figure 3A**). Results with G-36, **8**, and **21** show that there was a return to basal levels of cAMP by blocking the activation of the receptor with the experimentally determined cAMP EC_{80} value of GPER activation with agonist, G-1 (EC_{80}= 3 μM) (**Figure 3B**).

Selectivity of 8 and 21 for GPER over the classical ER

Due to the existence of multiple targets for estrogenic compounds, the selectivity of **8** and **21** for GPER over the classical ER was established. Unlike E_2, there was no appreciable binding for ERα observed by G-1, G-36, or **8** at any tested concentrations (**Figure 4A**). At the highest (10 μM) concentration evaluated, **21** showed a low level of binding that was significantly

Downloaded from www.jlr.org by guest, on March 8, 2020

different from G-1, G-36, and **8**. For this reason, **21** may be limited in effectiveness as a GPER antagonist due to the potential of off-target effects. Studies of ERβ binding revealed that at high (10 μM) concentrations, only G-1 and G-36 exhibited binding (**Figure 4B**). In contrast to the G-series, both **8** and **21** showed a lack of binding at the 10 μM concentration. Overall, binding studies revealed that both **8** and **21** do not exhibit significant binding to either ERα or ERβ at concentrations below 10 μM. Since **8** displayed greater selectivity at high concentrations compared to **21**, we have established **8** as the lead compound within this series. Henceforth, the compound **8 (**2-**C**yclohexyl-4-**I**sopropyl-*N*-(4-**M**ethoxy**B**enzyl)**A**niline) is referred to as **CIMBA**.

Prevention of estrogen-induced gallstones by CIMBA in OVX mice

Although inbred AKR/J mice have been found to be a gallstone-resistant strain, they are still susceptible to the formation of E_2-induced cholesterol gallstones (28). Notably, the inbred AKR/J strain expresses *Gper1*, *Erα*, and *Erβ* in the liver. To further explore whether GPER-selective antagonists play a key role in preventing the formation of estrogen-induced gallstones, CIMBA was first studied in OVX AKR/J mice fed a lithogenic diet and treated with exogenous E_2 at 6 μg/day for 8 weeks. **Figure 5A** shows that without treatment of CIMBA (i.e., at 0 μg/day/kg), 100% of E_2-treated OVX mice developed gallstones in response to being fed the lithogenic diet for 8 weeks. However, gallstone prevalence was significantly reduced from 80% to 40% in E_2-treated OVX mice receiving CIMBA from 16 to 32 μg/day/kg for 8 weeks. **Figure 5B** displays representative photomicrographs of amorphous mucin gel, liquid crystals, cholesterol monohydrate crystals, and gallstones in these mice, as observed by phase contrast and polarizing light microscopy. As shown in **Table 2**, the highest mole percent cholesterol and

Downloaded from www.jlr.org by guest, on March 8, 2020

JOURNAL OF LIPID RESEARCH ASBMB

cholesterol saturation index (CSI) value in pooled gallbladder bile were found in E_2-treated OVX mice receiving no CIMBA. In contrast, the mole percent of cholesterol in gallbladder bile was gradually reduced with an increase in doses of CIMBA. Thus, CSI values of pooled gallbladder bile were dramatically decreased from 1.61 to 1.23 by CIMBA (**Table 2**), which is consistent with a dose-dependent reduction in gallstone prevalence in E_2-treated OVX mice receiving various doses of CIMBA (**Figure 5A**). **Figure 5C** shows that without CIMBA treatment, the relative lipid composition of pooled gallbladder bile from E_2-treated OVX mice fed the lithogenic diet for 8 weeks is located in the central three-phase area denoted Region C on a taurocholate-rich bile phase diagram, in which the bile is composed mainly of solid cholesterol monohydrate crystals, liquid crystals, and saturated micelles (39). With an increase in doses of CIMBA, the relative lipid composition of pooled gallbladder bile progressively shifts downward and to the left of the phase diagram. These alterations are caused by a dramatic reduction in cholesterol content, a relative decrease in phospholipid content, and a relative increase in bile salt content (**Table 2**).

In addition, utilizing pooled liver tissues harvested from the mice used in the above gallstone studies, we found that CIMBA was absorbed into the liver at both doses as determined by HPLC/MS. When the doses of CIMBA treatment were augmented from 16 μg/day/kg to 32 μg/day/kg for 8 weeks, the concentrations of CIMBA in the liver were increased from 5 ng/g liver tissue to 25 ng/g liver tissue in OVX mice. Taken together, these results are consistent with a dose-dependent reduction in gallstone prevalence in E_2-treated OVX mice receiving CIMBA from 0 to 32 μg/day/kg (**Figure 5A**).

Figure 5D exhibits the effect of E_2 and CIMBA on the expression of *Gper1*, *Erα*, and *Erβ* in the liver. Compared to control OVX mice receiving neither E_2 nor CIMBA, hepatic

ASBMB JOURNAL OF LIPID RESEARCH

Downloaded from www.jlr.org by guest, on March 8, 2020

expression of *Gper1* was significantly increased in OVX mice treated with E_2 at 6 μg/day. However, expression of *Gper1* was significantly reduced by CIMBA in a dose-dependent manner. Of note, expression of *Erα* was significantly increased in three groups of OVX mice treated with E_2, regardless of whether mice received varying doses of CIMBA. As expected, expression of *Erβ* was slightly increased in all mice because its expression was approximately 50-fold lower compared to *Erα* in the mouse liver (28).

To investigate whether CIMBA protects against E_2-induced gallstone formation through the GPER pathway, we studied OVX ERα (-/-) mice fed the lithogenic diet and treated with exogenous E_2 at 6 μg/day for 8 weeks. Consistent with our published results (30), at 8 weeks on the lithogenic diet, 30% of OVX ERα (-/-) mice receiving no CIMBA (i.e., 0 μg/day/kg) suffered from E_2-induced gallstones (**Figure 6A**). However, under 8-week treatment of CIMBA at 32 μg/day/kg, no gallstones were detected in OVX ERα (-/-) mice, and only 40% of these mice formed mucin gel, liquid crystals, and cholesterol monohydrate crystals (**Figure 6B**). As shown in **Table 2**, the CSI value of pooled gallbladder bile was 0.84 in OVX ERα (-/-) mice treated with CIMBA at 32 μg/day/kg was markedly lower compared to that (CSI = 1.28) in OVX ERα (-/-) mice receiving no CIMBA. These results indicate that pooled gallbladder bile is unsaturated with cholesterol after 8-week treatment of CIMBA in OVX ERα (-/-) mice.

ASBMB JOURNAL OF LIPID RESEARCH

Downloaded from www.jlr.org by guest, on March 8, 2020

DISCUSSION

Despite the implication of estrogen and GPER in a variety of health and disease states, there has been limited clinical success with currently available GPER ligands. Although the G-series (G-1, G-15, and G-36) has become the standard for studies pertaining to GPER, the series may be limited by off-target effects and weak solubility in water or oil. A particular disadvantage of the G-series is the presence of ERE activation at high concentrations (18). To improve the solubility and address promiscuous binding of the G-series, we have rationally and successfully synthesized a new series of the GPER-selective antagonists that provide the first evidence for key binding interactions within the binding pocket of GPER.

Previously, our group explored binding interactions in a series of indole-thiazole derivatives that exhibited agonism at GPER (42). Molecular homology modeling found that the indole-thiazole derivatives exhibited π-π stacking similar to G-1 of the aromatic groups with F206$^{45.49}$ and F208$^{45.51}$ within the binding pocket of GPER (33, 34, 42). These results suggested that the tetrahydroquinoline is not required for GPER activity. Prior modifications of the G-series focused on site-selective alteration on the tetrahydroquinoline structure, but have not focused on additional substitution patterns. To explore the binding modes and interactions that are important for antagonism, the indole-thiazole scaffold has been revised. In the revised scaffold, the amide bond was replaced with an amine, and the heteroatoms of the indole-thiazole were changed to substituted benzene ring systems. We hypothesized that removal of the heteroatoms in the indole-thiazole would alter the pharmacological activity of the derivatives from agonists to antagonists. The structure of the G-series is similar in rigidity to estrogen and other steroids, which may contribute to weak solubility. Additionally, the lack of flexibility may reduce the

ASBMB JOURNAL OF LIPID RESEARCH

Downloaded from www.jlr.org by guest, on March 8, 2020

ability of GPER ligands to effectively probe the binding pocket. To address the concerns of the solubility and probing ability, the scaffold included more rotatable bonds than the G-series.

Using the hypothesized scaffold, we developed a simplistic route to synthesize the initial set of compounds (**5**–**25**) with varying substituents. The results of calcium mobilization studies show that the majority of the compounds in the series have the ability to antagonize the EC_{80} of the known GPER-selective agonist, G-1. Among these new series of compounds, CIMBA (**8**) and **21** display superior antagonism of the G-1 signaling activity in the HL-60 cell line. These two molecules have different substitutions at both the R_1 and R_2 positions of our scaffold, CIMBA (R_1 = isopropyl and R_2 = 4-OMe) and **21** (R_1 = *tert*-butyl and R_2 = 4-CH_3). At the R_1 substitution, it appears that GPER prefers bulkier hydrophobic groups, and varying the bulkiness of that groups influences the substitution pattern that is tolerated at the R_2 substitution. At the R_2 position, smaller electron donating groups are favored when R_1 is either an isopropyl or *tert*-butyl group. The electron donating nature of these two groups most likely contributes to the electron-rich aromatic ring, which influences either aryl–aryl or aryl–cation interactions (43). Trends in efficacy and potency were validated by evaluating cAMP. Overall, the findings from the current studies provide some critical insights into the binding interactions that can be utilized in the development of new ligands for modulating the GPER activity.

The selectivity studies show that CIMBA and **21** specifically bind GPER over ERα or ERβ below 10 μM. While CIMBA does not bind to either ERα or ERβ, **21** displays binding to ERα at 10 μM. These results are not surprising because the molecular modeling studies on GPER and the classical ER from our group and others are in agreement that estrogenic compounds bind within a similar binding pocket as each other (33, 34, 44-47). Due to the proposed similarity between the binding pockets for these three receptors, it is not surprising to observe off-target

Downloaded from www.jlr.org by guest, on March 8, 2020

ASBMB JOURNAL OF LIPID RESEARCH

binding by some GPER ligands at high concentrations (16-18). In our binding studies, we found that G-36 exhibits an increasing trend in binding at ERα. This is the first study to suggest potential off-target effects of G-36.

The results from this study show several key advantages of CIMBA over the G-series antagonists, G-15 and G-36. One advantage of CIMBA is the removal of the tetrahydroquinoline moiety. This could reduce potential off-target binding since these moieties are pan-assay interference compounds which generally lead to off-target effect, confusing structure-activity relationship of ligands, and poor downstream data (48, 49). Moreover, removing the tetrahydroquinoline moiety allows for less molecular rigidity and a greater ability to probe the GPER binding pocket. An additional advantage of CIMBA over G-15 and G-36 is that at high concentrations, CIMBA does not bind to either ERα or ERβ, thereby preventing induction of any ER-dependent ERE activation. Compared to the G-series antagonists, CIMBA also appears to be a more potent inhibitor of the calcium release induced by G-1. The increase in potency may be attributed to the increase in flexibility and the ability to probe the binding pocket of the receptor. Furthermore, CIMBA does not contain chiral centers that are present in G-1. The lack of chiral centers in CIMBA prevents a racemic mixture of both active and inactive stereoisomers, allowing for ease of synthesis and more accurate determination of potency. Lastly, CIMBA is more soluble than both G-15 and G-36 in 1% dimethyl sulfoxide (DMSO) solutions. In a preliminary study, we found that both G-15 and G-36 dissolve sparingly in water, oil, or alcohols. To be appropriately dissolved, G-15 and G-36 must be dissolved in a high concentration of DMSO. The restriction in solvents has limited the use of G-15 and G-36 in animal studies due to the significant cytotoxicity of DMSO. In contrast, CIMBA in the range of

ASBMB JOURNAL OF LIPID RESEARCH

Downloaded from www.jlr.org by guest, on March 8, 2020

pharmacological dosages can be dissolved in alcohol first and then oil so that it is convenient to be used for animal experiments through intramuscular, subcutaneous, or intraperitoneal injection.

As found by clinical and epidemiological studies, the prevalence of cholesterol gallstone disease in women is twice that of men (24), and oral contraceptives or other estrogen therapies significantly increase that risk (26). Although the classical ERα plays a critical role in estrogen-induced lithogenic effects, genetic studies have found that *Gper1* is a new gallstone gene, *Lith18*, in mice (31) and is also involved in estrogen-dependent lithogenic pathways (29, 50). In a mouse model of E_2-induced gallstones, CIMBA reduces gallstone formation in a dose-dependent manner in OVX mice. Of note, at the highest (32 μg/day/kg) concentration, CIMBA does not completely inhibit gallstone formation in OVX mice. One explanation for this observation is that even higher doses of CIMBA are needed to fully prevent E_2-induced gallstone formation. However, the most likely explanation is that since CIMBA does not bind to the classical ERs, ERα is still being activated by E_2, thus leading to gallstone formation (29). Using OVX ERα (-/-) mice, we further found that CIMBA protects against the formation of E_2-induced gallstones by inhibiting the *Gper1* activity in the liver. The current results are consistent with the findings reported in the literature (27), supporting the novel concept that GPER is involved in E_2-dependent lithogenic actions, working independently of ERα. These results also support the notion that both GPER and ERα can work through different pathways on hepatic cholesterol and bile salt metabolism, as well as biliary lipid secretion and cholesterol crystallization to promote E_2-induced cholesterol gallstones (29).

Taken together, the discovery of the potent GPER-selective antagonist, CIMBA, may provide a novel and alternative strategy for the prevention of cholesterol gallstones in women and, particularly for subjects who have to expose to high levels of estrogen. CIMBA is a

Downloaded from www.jlr.org by guest, on March 8, 2020

JOURNAL OF LIPID RESEARCH ASBMB

precedent for GPER antagonists to reduce GPER mRNA levels, as we found in the liver. Furthermore, CIMBA and the other compounds from this study also offer new pharmacological tools to evaluate the functions of GPER while exploring the ligand binding domain, which may greatly aid in the development of an orally administered, liver-specific, GPER-selective antagonist for the prevention of cholesterol gallstone disease in a subgroup of women at high risk.

ASBMB JOURNAL OF LIPID RESEARCH

Downloaded from www.jlr.org by guest, on March 8, 2020

Acknowledgments: This work was supported in part by the start-up funds from Saint Louis University (to CKA), as well as by research grants DK101793, DK106249, DK114516, and AA025737 (to DQ-HW), as well as P30 DK041296 (to Marion Bessin Liver Research Center), all from the National Institutes of Health (US Public Health Service).

Conflicts of interest: There is no conflict of interest for all authors.

ASBMB JOURNAL OF LIPID RESEARCH

Downloaded from www.jlr.org by guest, on March 8, 2020

REFERENCES

1. Heldring, N., A. Pike, S. Andersson, J. Matthews, G. Cheng, J. Hartman, M. Tujague, A. Ström, E. Treuter, M. Warner, and J.A. Gustafsson. 2007. Estrogen receptors: How do they signal and what are their targets. *Physiol. Rev.* **87**: 905-931.
2. Dahlman-Wright, K., V. Cavailles, S.A. Fuqua, V.C. Jordan, J.A. Katzenellenbogen, K.S. Korach, M. Muramatsu, M.G. Parker, and J.A. Gustafsson. 2006. International Union of Pharmacology. LXIV. Estrogen receptors. *Pharmacol. Rev.* **58**: 773-781.
3. Mosselman, S., J. Polman, and R. Dijkema. 1996. ERβ: Identification and characterization of a novel human estrogen receptor. *FEBS Letters*. **392**: 49-53.
4. Nilsson, S., S. Mäkelä, E. Treuter, M. Tujague, J. Thomsen, G. Andersson, E. Enmark, K. Pettersson, M. Warner, and J.A. Gustafsson. 2001. Mechanisms of estrogen action. *Physiol. Rev.* **81**: 1535-1365.
5. Kumar, R., B.H. Johnson, and E.B. Thompson. 2004. Overview of the structural basis for transcription regulation by nuclear hormone receptors. *Essays Biochem*. **40**: 27-39.
6. Matthews, J., and J.A. Gustafsson. 2003. Estrogen signaling: a subtly balance between ER alpha and ER beta. *Mol. Interv*. **3**: 281-292.
7. Marino, M., P. Galluzzo, P. Ascenzi. 2006;Estrogen Signaling Multiple Pathways to Impact Gene Transcription. *Curr. Genomics.* **7**: 497-508.
8. Filardo, E.J., J.A. Quinn, K.I. Bland, and A.R.J. Frackelton. 2000. Estrogen-induced activation of Erk-1 and Erk-2 requires the G protein-coupled receptor homolog, GPR30, and occurs via trans-activation of the epidermal growth factor receptor through release of HB-EGF. *Mol. Endocrinol.* **14**: 1649-1660.
9. Revankar, C.M., D.F. Cimino, L.A. Sklar, J.B. Arterburn, and E.R. Prossnitz. 2005. A transmembrane intracellular estrogen receptor mediates rapid cell signaling. *Science*. **307**: 1625-1630.
10. Levin, E.R.. 2001. Invited Review: Cell localization, physiology, and nongenomic actions of estrogen receptors. *J. Appl. Physiol*. **91**: 1860-1867.
11. Teskarik, J., and C. Mendoza. 1995. Nongenomic effects of 17 beta-estradiol on maturing human oocytes: relationship to oocyte developmental potential. *J. Clin. Endocrinol. Metab*. **80**: 1438-1443.
12. Aronica, S.M., W.L. Kraus, and B.S. Katzenellenbogen. 1994. Estrogen action via the cAMP signaling pathway: Stimulation of adenylate cyclase and cAMP-regulated gene transcription. *Proc. Natl. Acad. Sci. USA*. **91**: 8517-8521.
13. Kelly, M.J., and E.J. Wagner. 1999. Estrogen modulation of G-protein-coupled receptors. *Trends Endocrinol. Metab*. **10**: 369-374.
14. Migliaccio, A., M. Di Domenico, G. Castoria, A. de Falco, P. Bontempo, E. Nola, and F. Auricchio. 1996. Tyrosine kinase/p21ras/MAP-kinase pathway activation by estradiol-receptor complex in MCF-7 cells. *EMBO J.* **15**: 1292-1300.
15. Thomas, P., Y. Pang, E.J. Filardo, and J. Dong. 2005. Identity of an estrogen membrane receptor coupled to a G protein in human breast cancer cells. *Endocrinology*. **146**: 624-632.
16. Bologa, C.G., C.M. Revankar, S.M. Young, B.S. Edwards, J.B. Arterburn, A.S. Kiselyov, M.A. Parker, S.E. Tkachenko, N.P. Savchuck, L.A. Sklar, T.I. Oprea, E.R. Prossnitz. 2006. Virtual and biomolecular screening converge on a selective agonist for GPR30. *Nat. Chem. Biol.* **2**: 207-212.

ASBMB JOURNAL OF LIPID RESEARCH

Downloaded from www.jlr.org by guest, on March 8, 2020

17. Dennis, M.K., R. Burai, C. Ramesh, W.K. Petrie, S.N. Alcon, T.K. Nayak, C.G. Bologa, A. Leitao, E. Brailoiu, E. Deliu, N.J. Dun, L.A. Sklar, H.J. Hathaway, J.B. Arterburn, T.I. Oprea, and E.R. Prossnitz. 2009. In vivo effects of a GPR30 antagonist. *Nat. Chem. Biol.* **5**: 421-427.
18. Dennis, M.K., A.S. Field, R. Burai, C. Ramesh, W.K. Petrie, C.G. Bologa, T.I. Oprea, Y. Yamaguchi, S. Hayashi, L.A. Sklar, H.J. Hathaway, J.B. Arterburn, and E.R. Prossnitz. 2011. Identification of a GPER/GPR30 antagonist with improved estrogen receptor counterselectivity. *J. Steroid. Biochem. Mol. Biol.* **127**: 358-366.
19. Lappano, R., C. Rosano, M.F. Santolla, M. Pupo, E.M. De Francesco, P. De Marco, M. Ponassi, A. Spallarossa, A. Ranise, and M. Maggiolini. 2012. Two novel GPER agonists induce gene expression changes and growth effects in cancer cells. *Curr. Cancer Drug Targets.* **12**: 531-542.
20. Lappano, R., M.F. Santolla, M. Pupo, M.S. Sinicropi, A. Caruso, C. Rosano, and M. Maggiolini. 2012. MIBE acts as antagonist ligand of both estrogen receptor α and GPER in breast cancer cells. *Breast Cancer Res.* **14**: R12.
21. Maggiolini, M., M.F. Santolla, S. Avino, F. Aiello, C. Rosano, A. Garofalo, and F. Grande. 2015. Identification of two benzopyrroloxazines acting as selective GPER antagonists in breast cancer cells and cancer-associated fibroblasts. *Future Med. Chem.* **7**: 437-448.
22. Lappano, R., C. Rosano, A. Pisano, M.F. Santolla, De E.M. Francesco, P. De Marco, V. Dolce, M. Ponassi, L. Felli, G. Cafeo, F.H. Kohnke, S. Abonante, and M. Maggiolini. 2015. A calixpyrrole derivative acts as an antagonist to GPER, a G-protein coupled receptor: mechanisms and models. *Dis. Model Mech.* **8**: 1237-1246.
23. Papalia, T., R. Lappano, A. Barattucci, A. Pisano, G. Bruno, M.F. Santolla, S. Campagna, P. De Marco, F. Puntoriero, E.M. De Francesco, C. Rosano, M. Maggiolini, and P. Bonaccorsi. 2015. A Bodipy as a luminescent probe for detection of the G protein estrogen receptor (GPER). *Org. Biomol. Chem.* **13**: 10437-10441.
24. Wang, D.Q., and N.H. Afdhal: Gallstone Disease. In: Feldman M, Friedman LS, Brandt L, eds. Sleisenger and Fordtran's Gastrointestinal and Liver Disease. 10 ed. Philadelphia: Elsevier Saunders, 2014; 1100-1133.
25. Portincasa, P., A.D. Ciaula, L. Bonfrate, and D.Q. Wang. 2012. Therapy of gallstone disease: What it was, what it is, what it will be. *World J Gastrointest Pharmacol Ther.* **3**: 7-20.
26. Cirillo, D.J., R.B. Wallace, R.J. Rodabough, P. Greenland, A.Z. LaCroix, M.C. Limacher, and J.C. Larson. 2005. Effect of estrogen therapy on gallbladder disease. *JAMA.* **293**: 330-339.
27. Wang, D.Q., and P. Portincasa. Gallstones: Recent advance in epidemiology, pathogenesis, diagnosis and management. New York: Nova Biomedical, 2017: 1-676.
28. Wang, H.H., N.H. Afdhal, and D.Q. Wang. 2004. Estrogen receptor alpha, but not beta, plays a major role in 17beta-estradiol-induced murine cholesterol gallstones. *Gastroenterology.* **127**: 239-249.
29. de Bari, O., T.Y. Wang, M. Liu, P. Portincasa, and D.Q. Wang. 2015. Estrogen induces two distinct cholesterol crystallization pathways by activating ERalpha and GPR30 in female mice. *J. Lipid Res.* **56**: 1691-1700.
30. de Bari, O., H.H. Wang, P. Portincasa, M. Liu, and D.Q. Wang. 2015. The deletion of the estrogen receptor alpha gene reduces susceptibility to estrogen-induced cholesterol cholelithiasis in female mice. *Biochim. Biophys. Acta.* **1852**: 2161-2169.

ASBMB JOURNAL OF LIPID RESEARCH

Downloaded from www.jlr.org by guest, on March 8, 2020

31. Wang, T.Y., P. Portincasa, M. Liu, P. Tso, and D.Q. Wang. 2018. Mouse models of gallstone disease. *Curr. Opin. Gastroenterol.* **34**: 59-70.
32. Wang, H.H., M. Liu, D.J. Clegg, P. Portincasa, and D.Q. Wang. 2009. New insights into the molecular mechanisms underlying effects of estrogen on cholesterol gallstone formation. *Biochim. Biophys. Acta.* **1791**: 1037-1047.
33. Arnatt, C.K., and Y. Zhang. 2013. G protein-coupled estrogen receptor (GPER) agonist dual binding mode analyses toward understanding of its activation mechanism: A comparative homology modeling approach. *Mol. Inform.* 32:647-658.
34. Arnatt, C.K., and Y. Zhang: Chapter 7. A nuclear G protein-coupled estrogen receptor, GPER. homology modeling studies toward its ligand-binding mode characterization. In: Computational Approaches to Nuclear Receptors: The Royal Society of Chemistry, 2012; 117-137.
35. Wang, D.Q., B. Paigen, and M.C. Carey. 1997. Phenotypic characterization of Lith genes that determine susceptibility to cholesterol cholelithiasis in inbred mice: physical-chemistry of gallbladder bile. *J. Lipid Res.* **38**: 1395-1411.
36. Wang, H.H., X. Li, S.B. Patel, and D.Q. Wang. 2016. Evidence that the adenosine triphosphate-binding cassette G5/G8-independent pathway plays a determinant role in cholesterol gallstone formation in mice. *Hepatology*. **64**: 853-864.
37. Carey, M.C. 1978. Critical tables for calculating the cholesterol saturation of native bile. *J. Lipid Res.* **19**: 945-955.
38. Wang, D.Q., F. Lammert, D.E. Cohen, B. Paigen, and M.C. Carey. 1999. Cholic acid aids absorption, biliary secretion, and phase transitions of cholesterol in murine cholelithogenesis. *Am. J. Physiol.* **276**: G751-760.
39. Wang, D.Q., and M.C. Carey. 1996. Complete mapping of crystallization pathways during cholesterol precipitation from model bile: influence of physical-chemical variables of pathophysiologic relevance and identification of a stable liquid crystalline state in cold, dilute and hydrophilic bile salt-containing systems. *J. Lipid Res.* **37**: 606-630.
40. Lee, M.Y., J. Mun, J.H. Lee, S. Lee, B.H. Lee, and K.-S. Oh. 2014. A comparison of assay performance between the calcium mobilization and the dynamic mass redistribution technologies for the human urotensin receptor. *Assay Drug Dev. Technol.* **12**: 361-368.
41. Noblin, D.J., R.L. Bertekap, N.T. Burford, A. Hendricson, L. Zhang, R. Knox, M. Banks, J. O'Connell, and A. Alt. 2012. Development of a high-throughput calcium flux assay for identification of all ligand types including positive, negative, and silent allosteric modulators for G protein-coupled receptors. *Assay Drug Dev. Technol.* **10**: 457-467.
42. O'Dea, A., C. Sondergard, P. Sweeney, and C.K. Arnatt. 2018. A series of indole-thiazole derivatives act as GPER agonists and inhibit breast cancer cell growth. *ACS Med. Chem. Lett.* **9**: 901-906.
43. Bissantz, C., B. Kuhn, and M. Stahl. 2010. A medicinal chemist's guide to molecular interactions. *J. Med. Chem.* **53**: 5061-5084.
44. Mendez-Luna, D., M. Martinez-Archundia, R.C. Maroun, G. Ceballos-Reyes, M.J. Fragoso-Vazquez, D.E. Gonzalez-Juarez, and J. Correa-Basurto. 2015. Deciphering the GPER/GPR30-agonist and antagonists interactions using molecular modeling studies, molecular dynamics, and docking simulations. *J. Biomol. Struct. Dyn.* **33**: 2161-2172.
45. Rosano, C., M. Ponassi, M.F. Santolla, A. Pisano, L. Felli, A. Vivacqua, M. Maggiolini, and R. Lappano. 2016. Macromolecular modelling and docking simulations for the discovery of selective GPER ligands. *AAPS J.* **18**: 41-46.

JOURNAL OF LIPID RESEARCH ASBMB
Downloaded from www.jlr.org by guest, on March 8, 2020

46. Moreno-Ulloa, A., D. Mendez-Luna, E. Beltran-Partida, C. Castillo, G. Guevara, I. Ramirez-Sanchez, J. Correa-Basurto, G. Ceballos, and F. Villarreal. 2015. The effects of (−)-epicatechin on endothelial cells involve the G protein-coupled estrogen receptor (GPER). *Pharmacol. Res.* **100**: 309-320.
47. Vidad, A.R., S. Macaspac, and H.L. Ng. Locating the ligand binding sites for the G-protein coupled estrogen receptor (GPER) using combined information from docking and sequence conservation. bioRxiv 2016.
48. Baell, J.B. 2010. Observations on screening-based research and some concerning trends in the literature. *Future Med. Chem.* **2**: 1529-1546.
49. Baell, J.B., and G.A. Holloway. 2010. New substructure filters for removal of pan assay interference compounds (PAINS) from screening libraries and for their exclusion in bioassays. *J. Med. Chem.* **53**: 2719-2740.
50. Zucchetti, A.E., I.R. Barosso, A.C. Boaglio, C.L. Basiglio, G. Miszczuk, M.C. Larocca, M.L. Ruiz, C.A. Davio, M.G. Roma, F.A. Crocenzi, and E.J. Pozzi. 2014. G-protein-coupled receptor 30/adenylyl cyclase/protein kinase A pathway is involved in estradiol 17ß-d-glucuronide-induced cholestasis. *Hepatology*. **59**: 1016-1029.

ASBMB JOURNAL OF LIPID RESEARCH

Downloaded from www.jlr.org by guest, on March 8, 2020

Table 1. IC_{50} values of the inhibition of calcium mobilization in the HL-60 cells endogenously expressing the *Gper1* gene.

	R_1	R_2	IC_{50} (nM)
G-15	-	-	1,550 ± 170
G-36	-	-	1,350 ± 220
5	Isopropyl	Napthyl	260 ± 110
6	Isopropyl	4-Phenyl	191 ± 74
7	Isopropyl	4-CH_3	131 ± 21
8[#]	Isopropyl	4-OMe	75.0 ± 13.7
9	Isopropyl	4-H	>10,000
10	Isopropyl	4-Cl	197 ± 43
11	Isopropyl	3,4-Cl	255 ± 102
12	Methyl	Napthyl	338 ± 22
13	Methyl	4-Phenyl	365 ± 65
14	Methyl	4-CH_3	>10,000
15	Methyl	4-OMe	949 ± 28
16	Methyl	4-H	>10,000
17	Methyl	4-Cl	167 ± 17
18	Methyl	3,4- Cl	2,050 ± 780
19	*Tert*-butyl	Napthyl	>10,000
20	*Tert*-butyl	4-Phenyl	132 ± 145
21	*Tert*-butyl	4-CH_3	60.8 ± 18.0
22	*Tert*-butyl	4-OMe	874 ± 49

Downloaded from www.jlr.org by guest, on March 8, 2020

ASBMB JOURNAL OF LIPID RESEARCH

23	*Tert*-butyl	4-H	331 ± 160
24	*Tert*-butyl	4-Cl	141 ± 14
25	*Tert*-butyl	3,4-Cl	657 ± 94

G-15 and G-36 are displayed as a standard benchmark for GPER antagonism that can be used to compare **5**–**25**. The IC_{50} values are expressed as means ± SD. Each IC_{50} value is an average of three separate IC_{50} values obtained from triplicate measurements and the standard deviation is calculated from those three separate IC_{50} values. [#] This compound is later referred to as CIMBA.

Downloaded from www.jlr.org by guest, on March 8, 2020

Table 2. Lipid composition of gallbladder bile

E_2 (µg/day)	CIMBA (µg/day/kg)	Ch (*Mole%*)	PL (*Mole%*)	BS (*Mole%*)	Ch/PL Ratio	Ch/BS Ratio	Total Lipid Concentration (*g/dL*)	CSI
OVX AKR/J mice								
6	0	10.19	17.69	72.12	0.58	0.14	9.82	1.61
6	16	8.89	16.90	74.22	0.53	0.12	9.70	1.46
6	32	7.00	15.46	77.54	0.45	0.09	10.01	1.23
OVX ERα (-/-) mice								
6	0	7.38	15.85	76.78	0.47	0.10	9.72	1.28
6	32	4.48	14.22	81.30	0.31	0.06	10.50	0.84

Values were determined from pooled gallbladder bile (n=10 per group) in ovariectomized (OVX) mice fed the lithogenic diet for 8 weeks.

Abbreviations: Ch, cholesterol; CSI, cholesterol saturation index; BS, bile salts; E_2, 17β-estradiol; PL, phospholipids.

Downloaded from www.jlr.org by guest, on March 8, 2020

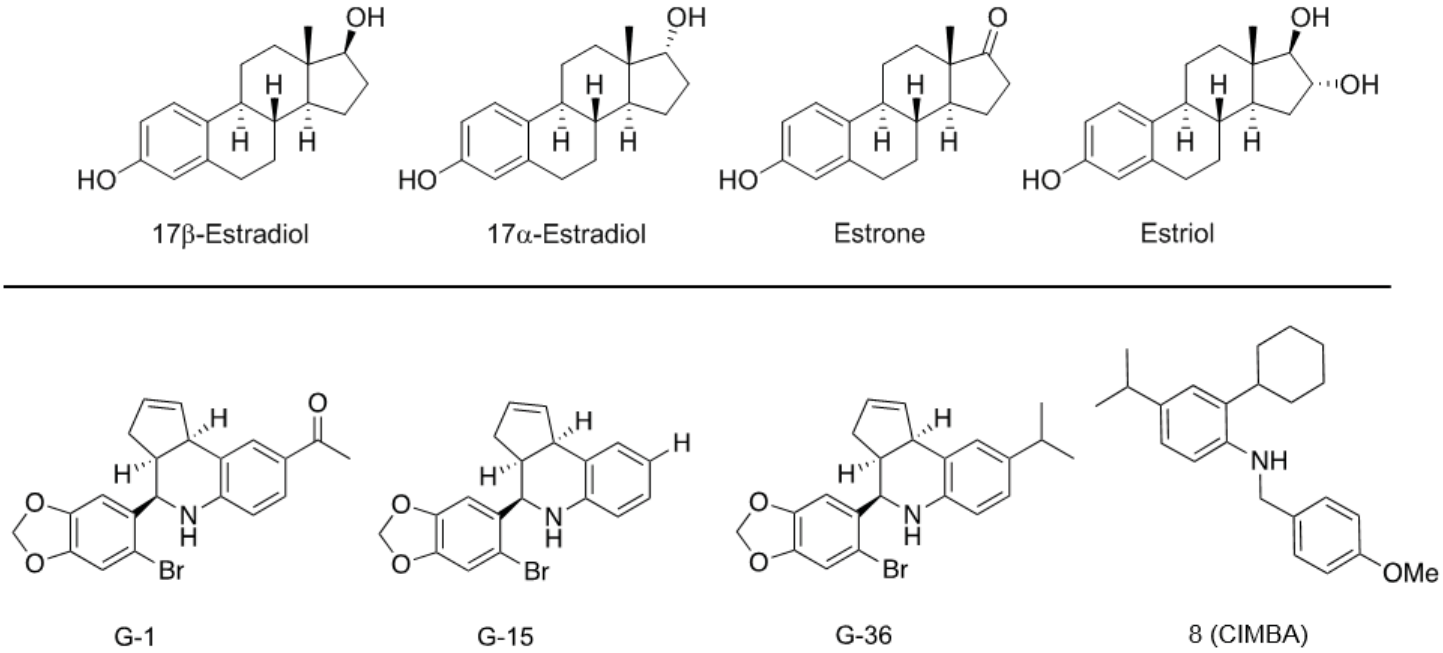

Figure 1. The endogenous ligand of GPER has been identified as 17β-estradiol (E_2). Other estrogenic compounds, 17α-estradiol, estrone, and estriol, all exhibit weak binding at GPER. *In silico* screening identified G-1 as a GPER-selective compound. Site-specific removal of the ethanone moiety (G-15) resulted in a change in pharmacological activity. G-15 exhibited off-target binding at the classical nuclear estrogen receptors, ERα and ERβ, and was further modified with an isopropyl moiety. The resulting compound G-36 exhibited a similar efficacy to G-15 but did not show off-target binding. This study identifies 8 (CIMBA) that can prevent the formation of estrogen-induced gallstones in female mice.

Downloaded from www.jlr.org by guest, on March 8, 2020

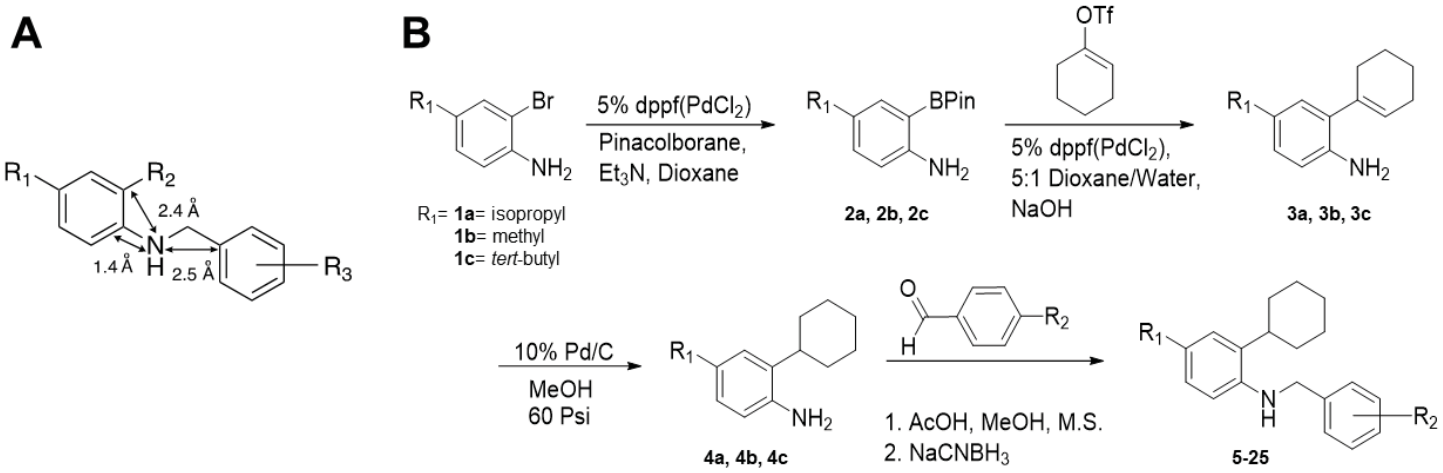

Figure 2. (**A**) The proposed scaffold consists of two benzene rings connected via a secondary amine linker. One of these benzene rings is intended to interact with F208 (EL2) and H307$^{7.37}$ and the other is meant to hold two hydrophobic moieties, R_1 and R_2, to interact with the hydrophobic pocket. The secondary amine linker is anticipated to hydrogen bond to N310$^{7.40}$, and varying substituents at R_3 have been included to explore the binding pocket in that region. (**B**) Because all brominated anilines (isopropyl, methyl, and *tert*-butyl) are available commercially, they serve as a logical starting point for the synthesis. The brominated anilines undergo Pd-catalyzed Miyaura Borylation with pinacolborane to produce borylated anilines (**2a, 2b,** and **2c**). The reaction of 1-cyclohexenyl trifluoromethansulfonate successfully couples to the borylated anilines to form **3a, 3b,** and **3c**. Catalytic hydrogenation of the coupled cyclohexenyl ring is afforded quantitatively in 10% Pd/C and H_2 to give **4a, 4b,** and **4c**. The final step of the synthetic route involves the reductive amination between the prepared aniline (**4a, 4b,** and **4C**) and various aldehydes (R_2) to yield **5**–**25**. The aldehydes are chosen to study variation in size and electrostatic properties that may be favorable within the binding pocket of GPER.

Downloaded from www.jlr.org by guest, on March 8, 2020

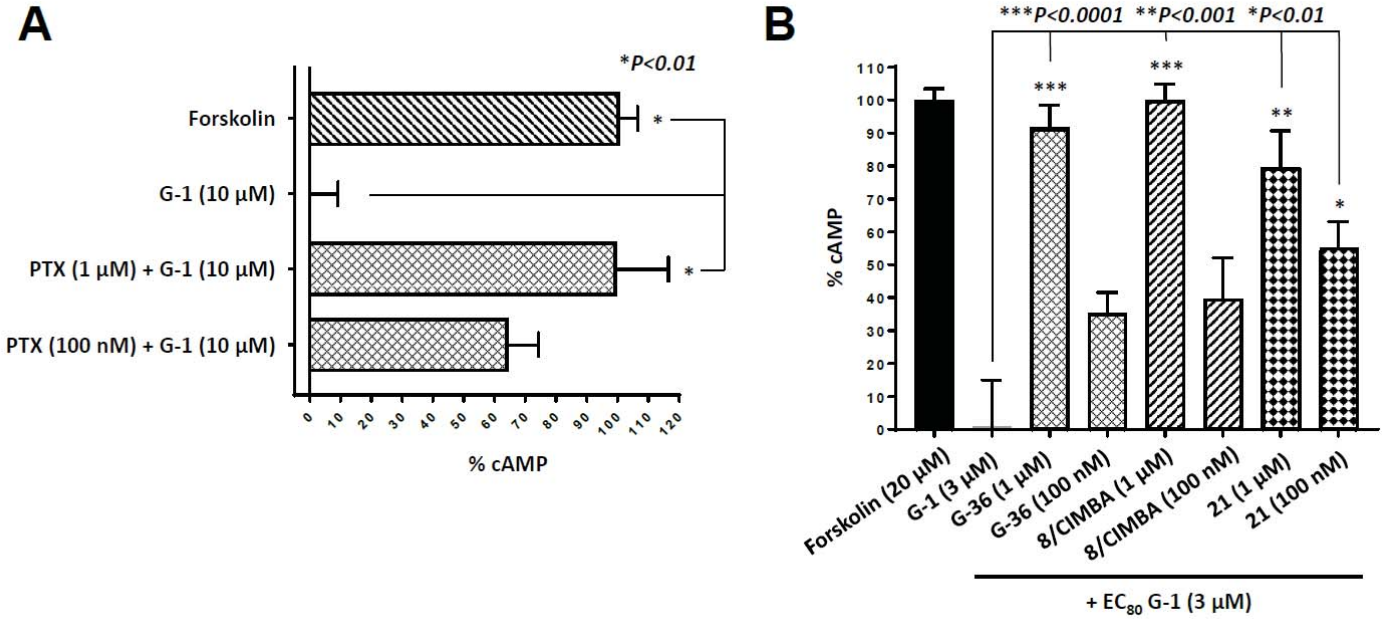

Figure 3. (**A**) A homogenous time-resolved fluorescence (HTFR) assay was used to determine the cAMP accumulation. Forskolin was utilized as a positive control for elevated levels of cAMP. HTRF values for compounds were normalized to the average signal obtained from forskolin (20 µM) to determine the %cAMP using the manufacturer's suggested protocols. The observed decrease in cAMP for 10 µM of G-1 was blocked with the use of 1 µM of pertussis-toxin (PTX) that inhibits the $G_{i/o}$ signaling pathway. (**B**) Compounds **8 (CIMBA)** and **21** were compared to a known GPER antagonist, G-36, and all three compounds exhibited the ability to antagonize the EC_{80} (3 µM) of G-1-induced inhibition of adenylate cyclase. At 1 µM exposure, **8 (CIMBA)** exhibited a similar level of inhibition (*$p<0.0001$, one-way ANOVA, Tukey's multiple comparison)* in response to the EC_{80} of G-1. Compound **21** exhibited a less statistically significant inhibition (*$p<0.001$).* A trend in inhibition of adenylate cyclase was also observed at 100 nM in these three compounds, but only **21** exhibited a significance (*$p<0.01$)* compared to the EC_{80} of G-1. All measurements were done in triplicate.

Downloaded from www.jlr.org by guest, on March 8, 2020

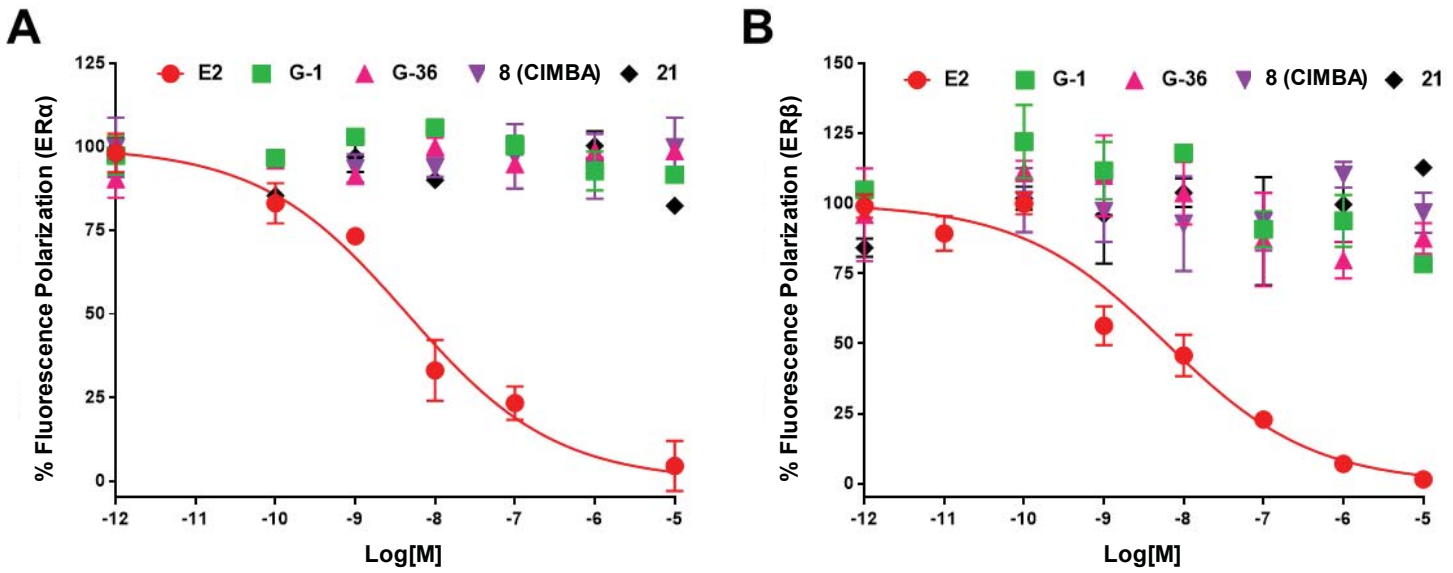

Figure 4. A fluorescence polarization binding assay was utilized to assess off-target binding of G-1, G-36, **8** (CIMBA), and **21** at ERα and ERβ. Data was compared to the binding of 17β-estradiol (E_2), a known ligand for both receptors. (**A**) At ERα, no appreciable binding was observed for G-1, G-36, and **8** (CIMBA) up to 10 μM. At the same concentration, **21** exhibited significant binding. (**B**) At ERβ, no binding was observed for either **8** (CIMBA) or **21** at 10 μM. At 10 μM, there was evidence of binding of G-1 to ERβ, and G-36 appeared to have a greater affinity at 10 μM than either 8 (CIMBA) or 21.

Downloaded from www.jlr.org by guest, on March 8, 2020

JOURNAL OF LIPID RESEARCH ASBMB

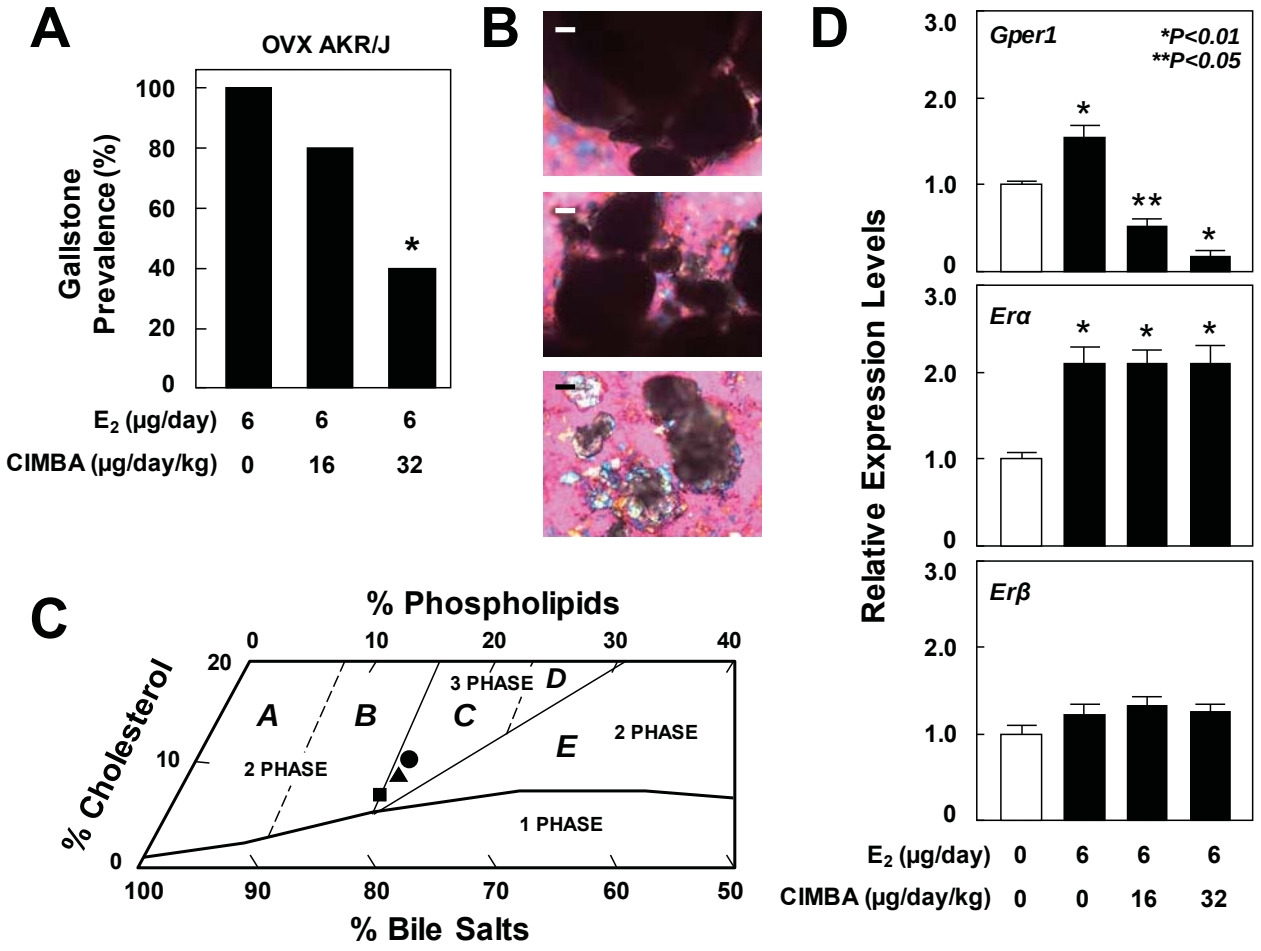

Figure 5. Effects of the potent GPER-selective antagonist, CIMBA, on the prevention of E_2-induced cholesterol gallstones. (**A**) CIMBA significantly reduces, in a dose-dependent manner, gallstone formation in E_2-treated OVX AKR/J mice (n=10 per group) fed the lithogenic diet for 8 weeks. (**B**) Representative photomicrographs of mucin gels, liquid crystals, cholesterol monohydrate crystals, sandy stones, and real gallstones as observed by polarizing light microscopy in gallbladder bile of E2-treated OVX mice (n=10 per group) at week 8 of feeding the lithogenic diet and treating with CIMBA at 0 (top panel; bar = 200 μm), 16 (middle panel; bar = 200 μm), or 32 μg/day/kg (bottom panel; bar = 100 μm). (**C**) The relative lipid composition of pooled gallbladder bile (n=10 per group) from E_2-treated OVX mice injected intraperitoneally with various doses of CIMBA from 0 to 32 μg/day/kg, as well as fed the lithogenic diet for 8 weeks is plotted on a condensed phase diagram. Because of an 8-week feeding of the lithogenic diet, the relative lipid composition of pooled gallbladder bile from E_2-treated OVX mice receiving no CIMBA (i.e., at 0 μg/day/kg) is located in the central three-phase zone denoted Region C, where at equilibrium, the bile is composed mainly of solid cholesterol crystals, liquid crystals, and saturated micelles. By treating mice with varying doses of CIMBA, the relative lipid composition of pooled gallbladder bile gradually shifts down. These alterations explain that gallstone prevalence is reduced in these mice treated with CIMBA in a dose-dependent fashion. The relative lipid composition of pooled gallbladder bile from E_2-treated OVX mice after 8 weeks of feeding of the lithogenic diet and treating with CIMBA at the following doses: ● 0 μg/day/kg; ▲ 16 μg/day/kg; and ■ 32 μg/day/kg, is plotted on the condensed phase diagram. (**D**) Effects of E_2 and CIMBA on the expression of *Gper1*, *Erα*, and *Erβ* in the liver. The data are expressed relative to mRNA levels of *Gper1*, *Erα*, and *Erβ* in the liver of OVX AKR/J mice (n=4 per group) receiving neither E_2 nor CIMBA, as well as fed the lithogenic diet for 8 weeks, and their relative expression levels are set at 1. Treatment of E_2 at 6 μg/day results in a significant increase in mRNA levels of the liver *Gper1* and *Erα*, but not *Erβ*, genes in OVX mice. Notably, expression of *Erβ* is approximately 50-fold lower compared to *Erα* in the mouse liver (28). Importantly, expression of *Gper1* in the liver is significantly reduced by the GPER-selective antagonist, CIMBA, in a dose-dependent manner in OVX mice even treated with E_2.

Downloaded from www.jlr.org by guest, on March 8, 2020

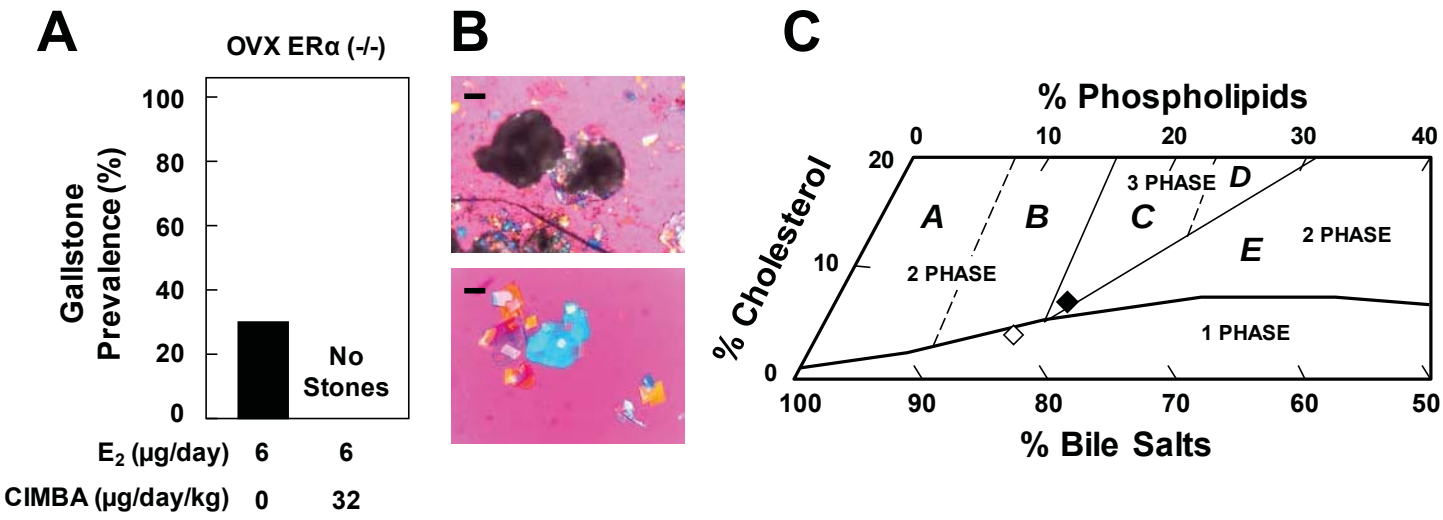

Figure 6. (**A**) After 8 weeks of feeding the lithogenic diet, E_2-induced gallstones are found in 30% of OVX ERα (-/-) mice (n=10) receiving no CIMBA. However, no gallstones are found in OVX ERα (-/-) mice (n=10) treated with CIMBA at 32 μg/day/kg, and only some mucin gels, liquid crystals, and cholesterol monohydrate crystals are detected in 40% of these mice. (**B**) Again, representative photomicrographs of mucin gels, liquid crystals, cholesterol monohydrate crystals, sandy stones, and real gallstones as observed in gallbladder bile of E2-treated OVX ERα (-/-) mice (n=10 per group) at week 8 of feeding the lithogenic diet and treating with CIMBA at 0 (top panel; bar = 200 μm) or 32 μg/day/kg (bottom panel; bar = 25 μm), as observed by polarizing light microscopy. (**C**) The relative lipid composition of pooled gallbladder bile from E_2-treated OVX ERα (-/-) mice fed the lithogenic diet, as well as treated with CIMBA at 0 (♦) or 32 μg/day/kg (◊) for 8 weeks is plotted on the condensed phase diagram.

Downloaded from www.jlr.org by guest, on March 8, 2020

ASBMB JOURNAL OF LIPID RESEARCH